Swirling Supersonic Nozzle Flow

J. C. Dutton*
University of Illinois at Urbana-Champaign, Urbana, Illinois

Swirling flow in supersonic propulsion nozzles has been investigated both numerically and experimentally. A time-dependent finite-difference technique has been developed and computations have been performed for a range of nozzle geometries, inlet swirl profiles, and swirl levels. The numerical results demonstrate that, while swirl has a minor effect on the specific impulse efficiency, relatively large reductions in the discharge coefficient and vacuum stream thrust efficiency have been computed at high swirl. For conventional converging and converging-diverging (c-d) nozzles, the major effect of swirl on the flowfield is to cause large increases in the axial velocity near the centerline, while the effects at the wall are much less pronounced. Good agreement between numerical and experimental wall static pressure distributions has been found for a c-d nozzle under nonswirling and two swirling flow conditions.

Introduction

SWIRLING flow in nozzles occurs in a number of important propulsion applications, including the flow in turbofan and turbojet engines, spin-stabilized rockets, and integral rocket/ramjets. In the first two cases, the tangential velocity component is induced by the motion of the turbine blades and by the rocket spin, respectively. For ramjets, recent experimental studies[1] have demonstrated that the swirl generated by fixed vanes located in the dump combustor inlet can lead to significantly improved combustor performance. Clearly, the swirl generated upstream in each of these propulsion systems will persist at some level to the inlet of the exhaust nozzle. Therefore, it is important that the effect of the tangential velocity component on the nozzle flowfield be known so that design parameters such as thrust and mass flow rate can be accurately determined.

The majority of previous investigations of swirling nozzle flow have been quasi-one-dimensional theoretical studies (see Refs. 2 and 3 for reviews of early work). Each of these investigations is limited to specific swirl velocity distributions and most also assume uniform stagnation pressure and temperature distributions. Another shortcoming of the quasi-one-dimensional method is that it neglects the radial velocity component. However, in the propulsion systems mentioned above, the quasi-one-dimensional assumptions are not generally valid since nozzle geometrical constraints often result in highly nonuniform flowfields.

A few two-dimensional calculations for inviscid, swirling, converging-diverging (c-d) nozzle flow have been performed, although no similar computations for converging nozzles are known. Guderley and his colleagues[4] obtained an approximate numerical solution for transonic throat flow with swirl that provided a starting line for the method of characteristics analysis of the supersonic portion of the nozzle. Boerner et al.[5] developed approximate series solutions for both weakly and strongly swirling flow in the throat region of axisymmetric nozzles. In a later study, Pandolfi[6] obtained two-dimensional, time-dependent calculations of swirling flow in a c-d nozzle with and without a centerbody. In each case, a single level of swirl was considered and no thrust calculations were reported. Recently, Kornblum et al.[7] and Hoffman et al.[8] analyzed a particular annular nozzle geometry with assumed free vortex, constant angle, forced vortex, and Rankine vortex swirl profiles. In each case, a time-dependent numerical technique was used for the subsonic and transonic portions of the flowfield and the method of characteristics was employed for the supersonic portion.

Few experimental measurements of swirling nozzle flow have been performed. Norton et al.[9] and Dunlap[10] used a spinning test apparatus to measure, respectively, the mass flow reduction due to spin and the flowfield in the combustion chamber upstream from the nozzle. Sforzini and his coworkers[11,12] experimentally investigated swirling flow in

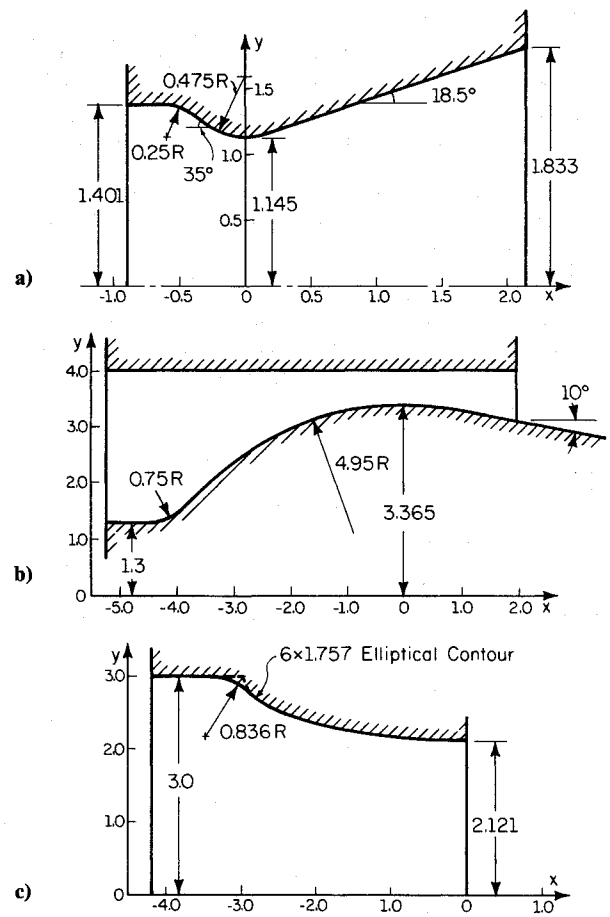

Fig. 1 Nozzle geometries analyzed in the numerical investigation: a) converging-diverging nozzle; b) annular nozzle; c) converging nozzle (arbitrary length units).

Received July 18, 1986; revision received Nov. 13, 1986.

*Associate Professor, Department of Mechanical and Industrial Engineering. Member AIAA.

single and multiple converging-diverging nozzles. For the case of a single nozzle, mass flow rate, thrust, and velocity profile data were obtained. Boerner et al.[5] obtained wall static pressure measurements for an annular nozzle that were compared with his series solutions. Qualitative agreement between the theoretical and experimental measurements was obtained. There are no previous data known for swirled nozzle flow generated by fixed or rotating vanes where the flow direction ahead of the vanes is predominantly axial, as occurs in ramjets and turbojets.

This paper presents the results of an integrated numerical and experimental investigation of the effects of swirl on propulsion nozzle performance and flowfield details. A time-dependent numerical technique has been developed and an extensive series of computations has been performed for several nozzle geometries, assumed tangential velocity distributions, and levels of swirl. In addition, experimental data obtained in a parallel effort is compared to the numerical results for a c-d nozzle for both unswirled and two swirling flows.

Numerical Investigation

Theoretical Formulation

In order to provide a uniformly valid solution for the entire subsonic/transonic/supersonic regions of the nozzle flowfield, the time-dependent numerical method has been employed. Under the assumptions of inviscid, non-heat conducting, axisymmetric flow of a thermally and calorically perfect gas, the appropriate governing equations can be written in nonconservative form as:

Continuity

$$\rho_t + u\rho_x + v\rho_y + \rho u_x + \rho v_y + \frac{\rho v}{y} = 0 \tag{1}$$

Euler equations

$$\text{Axial: } u_t + uu_x + vu_y + \frac{P_x}{\rho} = 0 \tag{2}$$

$$\text{Radial: } v_t + uv_x + vv_y - \frac{w^2}{y} + \frac{P_y}{\rho} = 0 \tag{3}$$

$$\text{Tangential: } w_t + uw_x + vw_y + \frac{vw}{y} = 0 \tag{4}$$

Energy

$$(P_t + uP_x + vP_y) - \frac{\gamma P}{\rho}(\rho_t + u\rho_x + v\rho_y) = 0 \tag{5}$$

where x and y are the axial and radial coordinates; u, v, and w the axial, radial, and tangential velocity components; and P, ρ, γ, t the pressure, density, specific heat ratio, and time, respectively. In this context, the term "axisymmetric" denotes that all derivatives in the tangential direction vanish, while the tangential velocity component does not. The inclusion of the w swirl velocity component requires the integration of the additional tangential Euler equation (4), as well as the appearance of the centripetal acceleration term w^2/y in the radial momentum equation (3). The result is a set of five coupled, nonlinear partial differential equations in five dependent variables: u, v, w, P, and ρ.

In order that the finite-difference calculations be performed on a rectangular grid, the governing equations are first transformed from (x, y, t) physical space to $(\zeta, \eta\, \tau)$ computational space, where the η coordinate varies from zero at the nozzle centerline (or centerbody wall) to unity at the outer wall and no transformation is performed on the axial coordinate or time. For conciseness, the transformed equations are not included here.

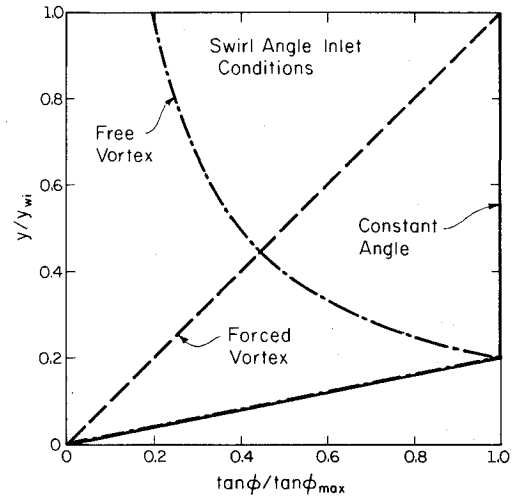

Fig. 2 Inlet swirl angle profiles used in the numerical investigation.

Numerical Technique

The approach adopted in this investigation has been to include the effects of swirl in an otherwise conventional time-dependent, nonswirling nozzle flow analysis. As a starting point, a version of the widely used NAP generation of codes written by Cline[13] has been used. These programs are well written and clearly documented and have been demonstrated to accurately and efficiently calculate nonswirling nozzle flows.

In the modified swirling nozzle program, the rectangular $\zeta-\eta$ computational plane is divided into equally spaced increments in the ζ and η directions, although $\Delta\zeta$ and $\Delta\eta$ are not necessarily equal. The interior points in the flowfield are calculated using MacCormack's[14] second-order accurate, explicit, predictor-corrector method. In order that an accurate evaluation of the boundary points be carried out, a reference plane characteristics scheme[13] has been used at *all* such points. For subsonic flow in the meridional plane at the nozzle inlet, the characteristics analysis demonstrates that only one compatibility equation is available, so that assumptions must be made about the values of four flow properties at each inlet point. After initial study,[15] the specified inlet properties have been taken as the stagnation pressure P_0, the stagnation temperature T_0, the meridian plane streamline angle $\theta \equiv \tan^{-1}(v/u)$, and the swirl angle $\phi \equiv \tan^{-1}(w/u)$. From a purely physical standpoint, it is likely that a reasonable assumption about the ϕ distribution can be made, especially when the swirl is generated by fixed or rotating vanes. The characteristics analysis also shows that for supersonic flow at the nozzle exit five compatibility equations must be simultaneously satisfied so that the exit flow properties are determined explicitly without resorting to extrapolation or assumptions about the outflow property distributions. Likewise, the wall and centerbody points are completely specified by four compatibility equations and the wall tangency boundary condition.

An additional point of interest regarding the numerical technique is that explicit artificial viscosity has not been included in any of the calculations reported herein. Further details concerning the theoretical formulation and numerical implementation may be found in Refs. 3, 13, and 15.

Numerical Results

Before proceeding to a discussion of the computed flowfields, the integral parameters used to judge the nozzle performance will be defined. Results have been obtained for the discharge coefficient C_D, the vacuum stream thrust efficiency η_{vs}, the specific impulse efficiency η_{SI}, and the nozzle

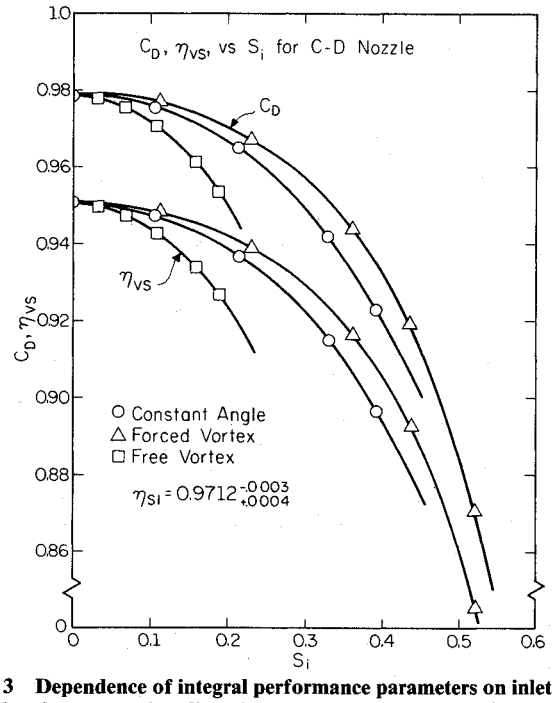

Fig. 3 Dependence of integral performance parameters on inlet swirl number for converging-diverging nozzle cases.

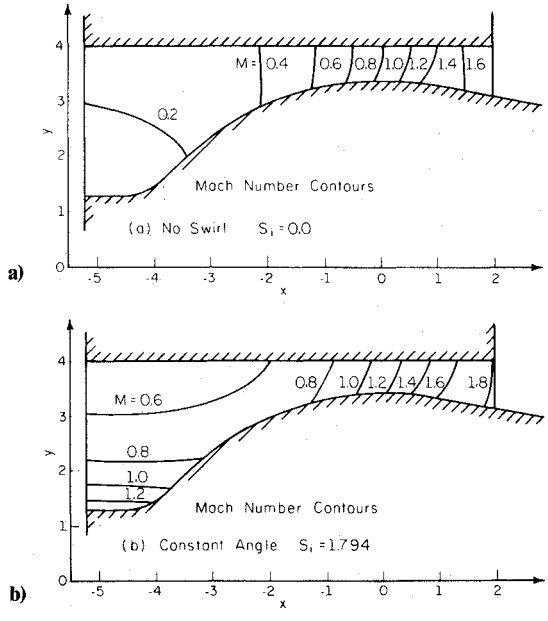

Fig. 4 Total Mach number contours for converging-diverging nozzle: a) no swirl; b) high swirl, constant-angle profile.

flowfield as functions of the inlet swirl number S_i, where

$$C_D \equiv \frac{\dot{m}}{\dot{m}_{id}} = 2\int_{y_c}^{y_w} \rho u y \mathrm{d}y \Big/ (y_{wt}^2 - y_{ct}^2)(\rho^* u^*)_{id} \tag{6}$$

$$\eta_{VS} \equiv \frac{T}{T_{id}} = 2\int_{y_{ce}}^{y_{we}} (P + \rho u^2) y \mathrm{d}y \Big/ (y_{we}^2 - y_{ce}^2)(P_e + \rho_e u_e^2)_{id} \tag{7}$$

$$\eta_{SI} \equiv \frac{(T/\dot{m})}{(T/\dot{m})_{id}} = \frac{\eta_{VS}}{C_D} \tag{8}$$

$$S_i \equiv \int_{y_{ci}}^{y_{wi}} \rho u w y^2 \mathrm{d}y \Big/ y_{wi} \int_{y_{ci}}^{y_{wi}} \rho u^2 y \mathrm{d}y \tag{9}$$

The subscripts *i, t, e, c, w,* and *id* are used to denote inlet, throat, exit, centerline or centerbody, wall, and ideal conditions, respectively, and $\dot{m}$ and T are the mass flow rate and vacuum stream thrust. The ideal conditions are defined as one-dimensional, isentropic values at the same stagnation conditions as the actual flow. As its name implies, η_{VS} is the thrust efficiency of a nozzle determined when both the actual and ideal flows are expanded to zero back pressure; as a measure of "internal" efficiency, η_{VS} is independent of the nozzle pressure ratio. Note that the inlet swirl number can be interpreted as the axial flux of flow angular momentum divided by the inlet wall radius times the axial flux of axial momentum and is, therefore, a measure of the level of swirl at the nozzle inlet.

Converging-Diverging Nozzle

The nozzle geometry used in the first series of computations is shown in Fig. 1a. It is a conventional converging-diverging nozzle with a cylindrical inlet, conical convergent and divergent sections, and circular arc transitions between these sections. The area contraction ratio between the nozzle inlet and throat is $A_t/A_i = 0.668$. This nozzle design is typical of those currently under development for ramjet systems. In addition, the nozzle inlet boundary conditions have been taken as P_0, T_0, and $\theta = 0$ uniform across the inlet, together with the three ϕ distributions shown in Fig. 2. Away from the centerline, $\tan\phi$ is constant for the "constant-angle" swirl profile and $\tan\phi$ is inversely proportional to y for the "free vortex" profile, while for the "forced vortex" profile $\tan\phi$ is directly proportional to y across the entire nozzle inlet. Note that since the axial velocity component u is not necessarily constant across the inlet with specified values of P_0, T_0, θ, and ϕ, these ϕ profiles do not necessarily translate directly into corresponding w tangential velocity profiles. A linear, forced vortex profile has been assumed in the centerline region for the constant-angle and free vortex profiles in order to enforce the $w = 0$ centerline symmetry condition. The radius ratio chosen for the matching point, $y/y_{wi} = 0.2$, is typical of that of the hub of fixed vane swirlers.[1] In addition, a specific heat ratio of $\gamma = 1.4$ has been used in these and all succeeding calculations.

Results for the discharge coefficient and vacuum stream thrust efficiency as a function of the inlet swirl number are shown in Fig. 3 for each of the assumed profiles. At given S_i, the reductions in C_D and η_{VS} are largest for the free vortex profile followed by the constant-angle and forced vortex profiles. The reason for this result is that, as will be shown shortly, the major effect of swirl on the nozzle flowfield is to cause a large increase in the axial velocity near the centerline. Since large values of ϕ_{max} are required in the centerline region to achieve a given S_i for the free vortex profile [see Fig. 2 and Eq. (9)], even moderate values of S_i result in a highly nonuniform throat flowfield due to the centerline sensitivity effect. This causes the steep decrease in C_D and η_{VS} as a function of S_i for the free vortex profile as compared to the constant-angle and forced vortex cases. Interestingly, the specific impulse efficiency η_{SI} is essentially constant for the entire range of cases shown in Fig. 3. This result suggests that for this geometry at fixed stagnation conditions, the reduction in thrust due to swirl is caused solely by the reduction in mass flow. For a constant mass flow device like a ramjet at supersonic flight conditions, on the other hand, the introduction of swirl entails essentially no loss in thrust, but rather results in an increased combustor pressure. To avoid this loss in mass flow and thrust or increased combustor pressure, the nozzle throat may be enlarged by the appropriate amount indicated in Fig. 3.

Total Mach number contours, $M \equiv (u^2 + v^2 + w^2)^{1/2}/a$, for an unswirled and swirled case are presented in Figs. 4a and 4b, respectively. The flowfield shown in Fig. 4a for the no swirl case is typical of that for a conical nozzle. Due to the relatively small wall radius of curvature, a strong expansion of the flow occurs in the throat wall region, which greatly lead the ex-

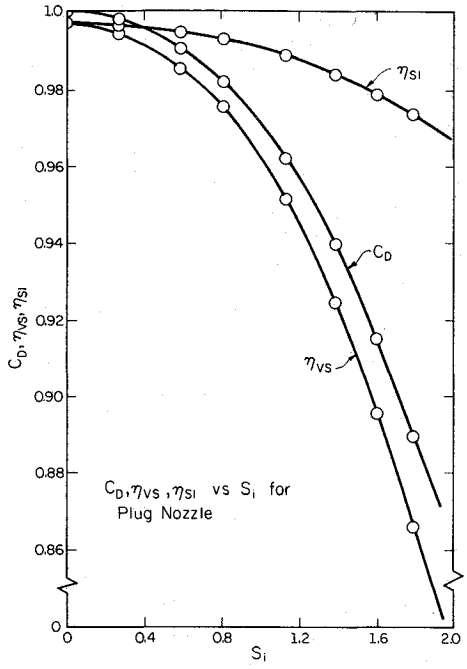

Fig. 5 Dependence of integral performance parameters on inlet swirl number for annular nozzle cases.

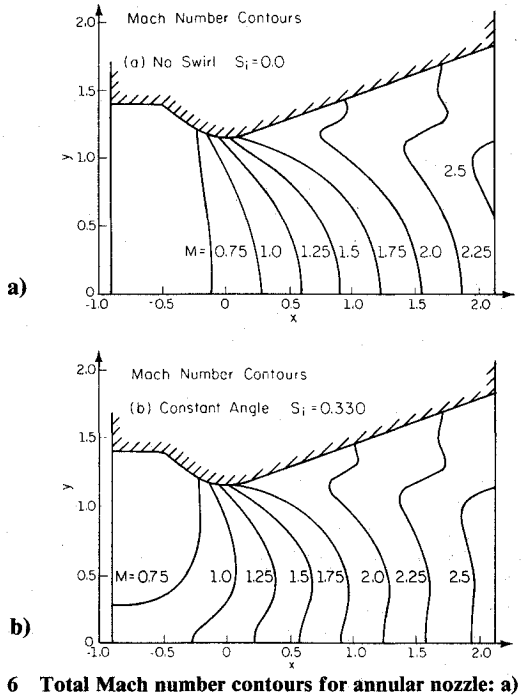

Fig. 6 Total Mach number contours for annular nozzle: a) no swirl; b) high swirl, constant-angle profile.

pansion occurring along the nozzle centerline. The difference in shape of the $M=2.0$ and 2.25 contours in the wall region compared to lower Mach number contours is due to an oblique shock wave which forms in the flowfield near the tangency point ($x=0.15$) between the circular arc throat and conical divergent wall sections. A discontinuity in the curvature of the wall contour occurs at this point, leading to Mach wave coalescence in this region. Comparing the unswirled case (Fig. 4a) to a highly swirled constant angle case (Fig. 4b), the most notable difference is seen to be an upstream shifting of the Mach number contours near the axis in Fig. 4b. In other words, the predominant effect of swirl on the nozzle flowfield is a large increase in the axial velocity near the centerline as

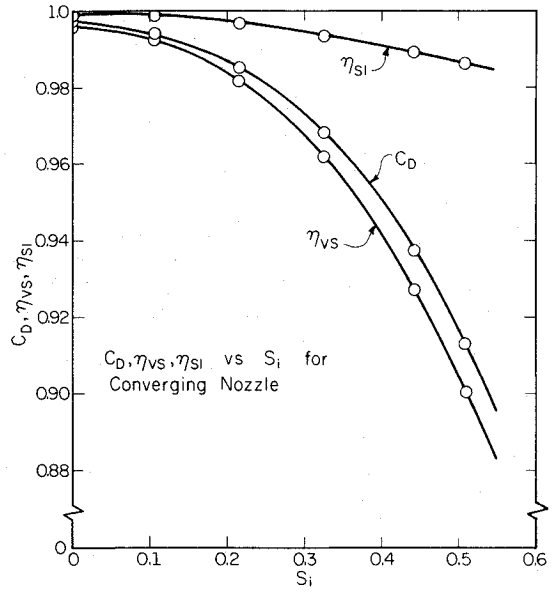

Fig. 7 Dependence of integral performance parameters on inlet swirl number for converging nozzle cases.

compared to the unswirled case. The influence of the tangential velocity component on the flowfield near the wall, on the other hand, is weak.

For an annular nozzle with free vortex, constant-angle, forced vortex, and Rankine vortex inlet swirl profiles, Hoffman et al.[8] computed decreases in the discharge coefficienct with swirl similar to those presented in Fig. 3. However, the Mach number distributions for the annular nozzle were influenced to a lesser degree by swirl than noted near the centerline for the conventional c-d nozzle reported here. In addition, rather than being constant, the specific impulse of the annular nozzle was found[8] to decrease with swirl for all four profiles considered. The latter result agrees with the computations of the next section.

Annular Nozzle

In order to demonstrate the ability to compute swirling flow in annular nozzles with centerbodies, the geometry shown in Fig. 1b has been analyzed. This is the turbojet plug nozzle investigated experimentally under nonswirl conditions by Bresnahan and Johns.[16] The outer wall is a straight, cylindrical one, while the inner wall has a cylindrical inlet, a circular arc transition to a circular arc throat, and a 10 deg conical plug section. The area contraction ratio in this case is $A_t/A_i = 0.327$. This geometry is interesting since the flowfield characteristics are quite different from those of the just discussed c-d nozzle. For the converging-diverging nozzle, the tangential velocity component along the wall increases from the inlet to the throat, then decreases to the exit as the wall radius first decreases, and then increases [conservation of angular momentum, Eq. (4)]. For the plug nozzle in Fig. 1b, however, w should be constant along the outer wall since its radius is constant; w should first decrease and then increase as the flow traverses from the inlet to the throat to the exit along the inner wall. The contraction in area from inlet to throat is also significantly larger for the annular nozzle than for the c-d nozzle. For the computations reported here, the boundary conditions have been taken as P_0, T_0, ϕ, and $\theta=0$ uniform across the entire inlet, i.e., a constant-angle swirl profile.

The results for the integral performance parameters as a function of the swirl level are presented in Fig. 5. Over the range of swirl numbers investigated, the reductions in the discharge coefficient and vacuum stream thrust efficiency as compared to the unswirled case are approximately 11 and 13%, respectively. These are the largest reductions computed

for any of the cases reported herein. In addition, the specific impulse efficiency is not constant as for the c-d nozzle, but rather decreases by 2.3% over the range of S_i computed. Also of interest is the magnitude of the swirl numbers along the abscissa in Fig. 5, values roughly four times those in Fig. 3 for the c-d nozzle. Because of the large contraction in area, which causes a large increase in the axial velocity from the inlet to throat, and because the tangential velocity decreases from the inlet to throat, the flow must be very strongly swirled at the plug nozzle inlet in order to have a significant effect on the performance parameters. In fact, for the most highly swirled case considered, the swirl velocity component is approximately 2.7 times the axial at the inlet, so that the tangential velocity is clearly the dominant component in this region.

Contours of constant total Mach number are plotted in Figs. 6a and 6b for the unswirled and a highly swirled case, respectively. The contours for the unswirled case are fairly uniform in the throat region due to the relatively large plug wall radius of curvature. The difference in shape of the $M=1.4$ and 1.6 contours is again due to a weak oblique shock that propagates into the flow from the region near the tangency point between the circular arc throat and 10 deg conical plug sections ($x=0.860$). For the highly swirled flow, the Mach number contours in the inlet region are vastly different from those for the no-swirl case. As the flow progresses along the inner wall near the inlet, the total Mach number actually *decreases* because the tangential velocity, which is the dominant component, is decreasing. As the throat is approached, however, the axial velocity eventually becomes the largest component, such that in the throat region the Mach number contours become more conventional in shape. Along the outer wall, both the unswirled and swirled flows experience a monotonic acceleration from subsonic to supersonic conditions. The outer wall Mach number distribution for the swirled case, however, everywhere exceeds that of the unswirled flow, especially in the inlet region.

Converging Nozzle

The converging nozzle geometry shown in Fig. 1c has a cylindrical inlet with a circular arc transition to an elliptically contoured converging section. This nozzle is nearly identical to the $A_t/A_i=0.5$ contraction ratio nozzle used in the Ramjet Technology Branch at Wright-Patterson Air Force Base in ramjet combustor experiments. The inlet boundary conditions used in this case are P_0, T_0, and $\theta=0$ uniform across the inlet and a constant-angle swirl profile similar to the one sketched in Fig. 2. The matching point between the linear and constant portions of the $\tan\phi$ profile, however, is located at $y/y_{wi}=0.214$ for these calculations. A portion of the swirling exhaust plume has been calculated in each case, such that the flow at all downstream boundary mesh points is supersonic in the meridional plane due to the aforementioned advantages of this exit condition. Iterative use of the wall point algorithm is employed to enforce the $P=P_{amb}$ boundary condition for the plume boundary points. A stagnation-to-ambient pressure ratio of 3.0 has been used in all of the results presented here. A few of the computations were repeated at $P_0/P_{amb}=5.0$ with virtually identical results, demonstrating the back pressure-independent nature of this flow.

The swirl number dependence of the performance quantities C_D, η_{vs}, and η_{SI} is plotted in Fig. 7. As for the previous cases, C_D and η_{vs} decrease rather rapidly with S_i, reaching values 8.5 and 9.6% less than for nonswirling flow at the highest swirl level investigated. In this instance, the specific impulse efficiency is not constant, but rather decreases slightly (approximately 1.3%) over the range of S_i studied. For the converging nozzle, the decay of C_D and η_{vs} with S_i is somewhat less rapid than for the previously discussed c-d nozzle. This is due primarily to the fact that the area contraction ratio for the converging nozzle is somewhat smaller than for the c-d nozzle, leading to a stronger acceleration of the axial velocity component from inlet to throat and, therefore, to reduced swirl effects when based on inlet conditions.

Unswirled and highly swirled total Mach number contours are plotted for this converging nozzle in Figs. 8a and 8b, respectively. In many respects, the comments made earlier with respect to the converging-diverging nozzle results also apply here. Comparing Figs. 8a and 8b, the most obvious difference is the strong upstream shift in the contours near the centerline for the swirled flow. Thus, as for the c-d nozzle, the flow experiences a smooth acceleration along the axis with the swirled case having significantly higher axial velocities at a given location than the unswirled case. At the nozzle wall, the effect of the tangential velocity component is minor by comparison. The relatively strong expansion occurring at the exit lip point is captured by the computations, as is the correct prediction of a constant total Mach number along the free jet boundary. Another interesting result is that, even at the highest level investigated, swirl has virtually no effect on the initial part of the plume shape.

Computational Details/Conservation Checks

As mentioned in the discussion of the numerical technique, the grids employed have equal spacing in both the axial and radial directions. Each of the previously discussed c-d nozzle calculations has been done on an 81×21 grid. Since the annular and converging nozzle geometries are somewhat less extreme with shorter supersonic flow sections, each of these nozzles was analyzed using a 41×15 grid. For each calculation, the initial value plane used was either an approximate one-dimensional plane calculated internally by the analysis code or the converged flowfield solution at the next lower level of swirl. The primary quantity used in monitoring convergence to steady state is the rms value over the grid of the fractional static pressure change from one time plane to the next $(\Delta P/P)_{rms}$. However, rather than continuing computations in the time domain until $(\Delta P/P)_{rms}$ falls to a specified value, Cline's suggestion[13] has been adoped that a fixed number of time planes be calculated to ensure that an "average" fluid particle passes through the computational domain at least five times. This time is computed by calculating the average velocity along a convenient streamline, such as at the nozzle centerline or wall, and dividing this velocity into the length of the streamline. After the required number of time planes (500–2000 for the results presented here), it is found that $(\Delta P/P)_{rms}$ has reached values on the order of 10^{-5} or less for each case, demonstrating convergence to steady state.

In order to thoroughly validate the computations, an extensive series of calculations of conserved quantities has been included in the code—these quantities have been monitored during the converging-diverging, annular, and converging nozzle calculations discussed previously. For inviscid, adiabatic, shockless flow, and assuming uniform stagnation pressure P_0 and stagnation temperature T_0 across the nozzle inlet, P_0 and T_0 should be constant through the entire flowfield at steady state. In addition, the axial distribution of mass flow rate $\dot{m}$ and the flow angular momentum along streamlines yw [integrated form of Eq. (4)] should be constant in steady flow. However, since these conservation conditions are not identically satisfied by the nonconservation form of the governing equations employed in the numerical technique, their calculation provides a self-check on the accuracy of the finite-difference computations.

In all of the cases investigated, P_0 and T_0 have been very constant in the flowfield, usually being within 0.1% of the prescribed values at the nozzle inlet. Likewise, mass flow and flow angular momentum are also well conserved in each case, with the fluctuations generally being less than $\pm0.5\%$ of the mean. Example conservation plots are shown in Fig. 9 for a highly swirled, constant-angle, converging-diverging nozzle calculation (geometry of Fig. 1a). The mass flow deviation, $\dot{m}/\dot{m}_{ave}-1$, is plotted as a function of the axial coordinate in Fig. 9a, while the wall angular momentum deviation, $yw/(yw)_{ave}-1$, is similarly plotted in Fig. 9b. In order to assess the effects of grid refinement, the original calculations

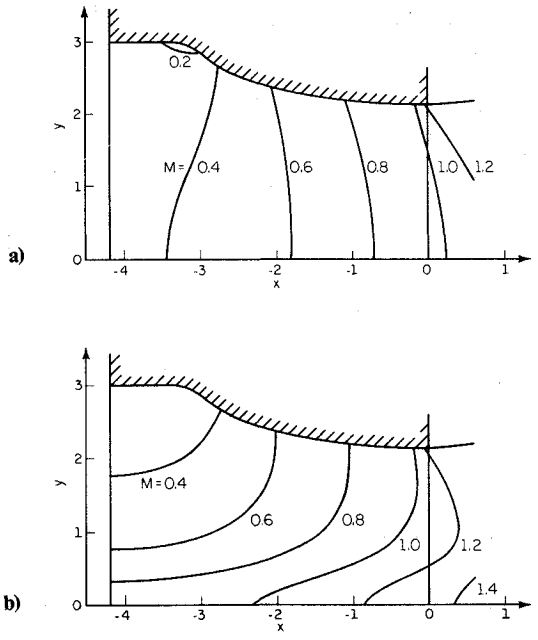

Fig. 8 Total Mach number contours for converging nozzle: a) no swirl; b) high swirl, constant-angle profile.

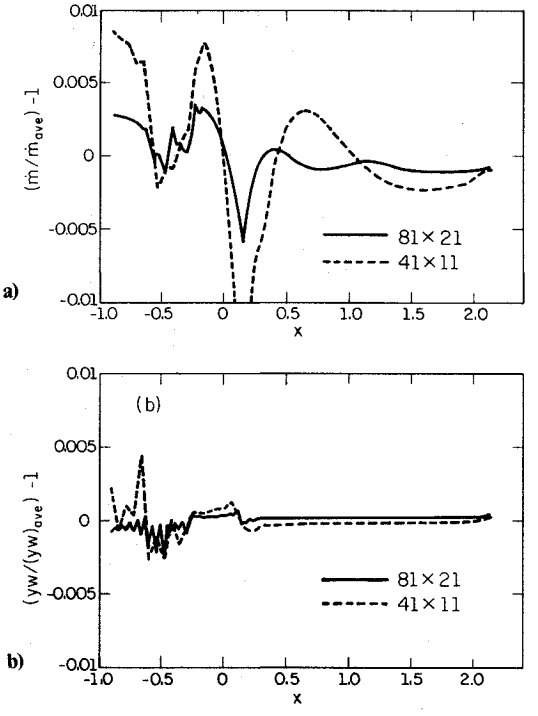

Fig. 9 Conservation plots for highly swirled, constant-angle, converging-diverging nozzle flow: a) mass flow; and b) wall angular momentum.

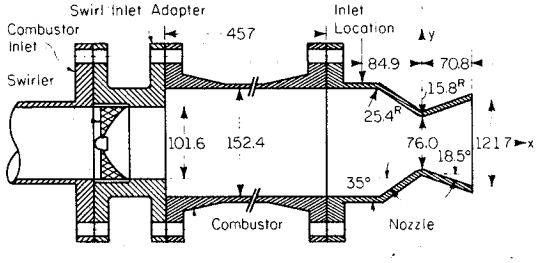

Fig. 10 Experimental swirler/dump combustor/converging-diverging nozzle facility (all dimensions in mm).

done on an 81×21 grid have been repeated using a coarser 41×11 grid. For both grids, the mass flow and particularly, the wall angular momentum are well conserved, although the 81×21 grid is clearly superior—as expected. The "spikes" occurring in the mass flow conservation plots appear near the tangency point between the circular arc throat and conical divergent sections where an oblique shock wave leads to strong flow property gradients. The results also demonstrate that the gross performance parameters, including C_D, η_{vs}, η_{SI}, and S_i, are within 0.15% of each other using the two grids. Further details concerning these computational checks can be found in Ref. 3.

Experimental Investigation

Experimental Apparatus

In order to provide a basis of comparison for the numerical calculations, wall static pressure measurements have been obtained from the Ramjet Technology Branch at Wright-Patterson Air Force Base[17] for swirling and nonswirling flow through a converging-diverging nozzle. A schematic of the test hardware is shown in Fig. 10. In all of these experiments, the c-d nozzle was mounted immediately downstream from a sudden enlargement (dump) combustor with a length-to-diameter ratio of $L/D=3$. The flowfield swirl was generated by fixed vane swirlers designed[1] to produce constant-angle profiles and located in the combustor inlet. The nozzle geometry is quite similar to the one discussed previously (Fig. 1a) with a cylindrical inlet, a circular arc transition to a 35 deg conical converging section, a circular arc throat, and an 18.5 deg conical divergent section. The contraction in area occurring between the nozzle inlet and throat is much larger in this case, i.e., $A_t/A_i=0.249$.

Cold, dry, compressed air was supplied to the combustor facility from centrifugal compressors; this air passed through the nozzle test section before entering the exhauster system. A five-hole Pitot probe was traversed across the nozzle inlet location shown in Fig. 10 in order to measure the inlet profiles of stagnation pressure and swirl angle. The wall static pressure distributions have been determined by means of 22 pressure taps located axially along the nozzle wall. Individual pressure transducers were connected to each of the wall static taps and the pressure data were acquired and reduced by means of a Mod Comp II minicomputer. Further details concerning the Ramjet Combustor Test Facility at WPAFB, its instrumentation, and data acquisition and reduction capabilities may be found in Ref. 1.

Experimental Results and Comparison to Computations

Wall static pressure data has been obtained for three cases: 1) no swirl; 2) moderate swirl, denoted by CA3 (constant angle $S=0.3$); and 3) high swirl, referred to as CA5 (constant angle $S=0.5$). In the swirler designation, the swirl number is the nominal design value based on Eq. (9) evaluated at the *swirler exit* not at the inlet to the nozzle. The boundary conditions used in the numerical calculations were T_0 and $\theta=0$ uniform across the nozzle inlet, together with the measured inlet distributions of P_0 and ϕ. The experimental inlet stagnation pressure profiles for the three cases and the swirl angle profiles for the two swirled cases are presented in Fig. 11. In each case, the flow has been probed from one wall, through the centerline, to the opposite wall, so that conclusions regarding the symmetry of the flow about the centerline can be drawn. As shown in Fig. 11a, the P_0 distributions are relatively symmetric for the three cases and, for the unswirled and moderately swirled cases, the variation in P_0 from the centerline to the nozzle wall is small ($<3\%$). Interestingly, however, the total pressure decreases from the centerline to the wall for the unswirled case while it increases for the two swirled flows. Also, the P_0 distribution is fairly nonuniform for the highly swirled case, approaching a 10% variation from the centerline to the wall. The swirl angle profiles in Fig. 11b are roughly symmetric about the centerline, except near the

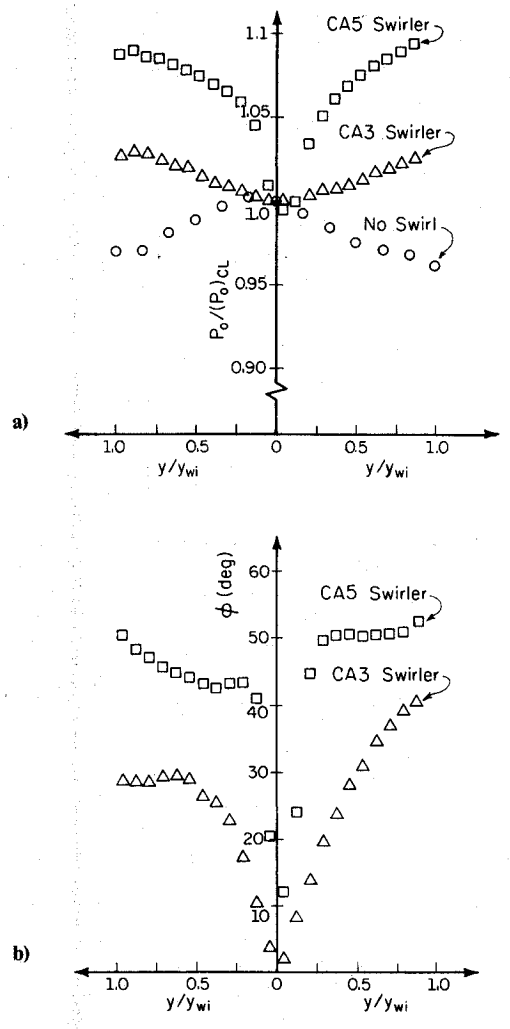

Fig. 11 Experimental inlet profiles for converging-diverging nozzle flow: a) stagnation pressure; b) swirl angle.

wall for the CA3 swirler. The measured ϕ asymmetries may be partially due to unequal probe blockage effects since the probe is always more than half inserted for one of the centerline-to-wall traverses and always less than half inserted for the other. These P_0 and ϕ distributions were used as input for the axisymmetric analysis code by averaging the two centerline-to-wall profiles for each case and using linear interpolation as necessary.

The experimental results presented in Fig. 11 provide needed information concerning assumptions that can be made for the inlet flow property distributions for swirling nozzle flow calculations. In particular, at least for the case in which the nozzle is just downstream from a relatively short dump combustor, the axisymmetric assumption is reasonable, although for highly swirled flow the uniform P_0 assumption may not be adequate.

Qualitatively, the Mach number contours computed for the three experimental cases (63×21 grid) are quite similar to those shown previously in Fig. 4 due to the similarities in the two nozzle designs. Comparing the axis and wall Mach number distributions calculated for the unswirled and CA3 swirler flows, it is found that the effect of swirl is significant only in the inlet region ($x \leq -10$ mm), although it is at least as large at the wall as at the centerline. In addition, the unswirled centerline Mach numbers are *larger* near the inlet than for the swirled flow. Although these results differ from those discussed previously, it must be remembered that the measured nonuniform profiles presented in Fig. 11a have been employed as the inlet P_0 boundary condition rather than assuming

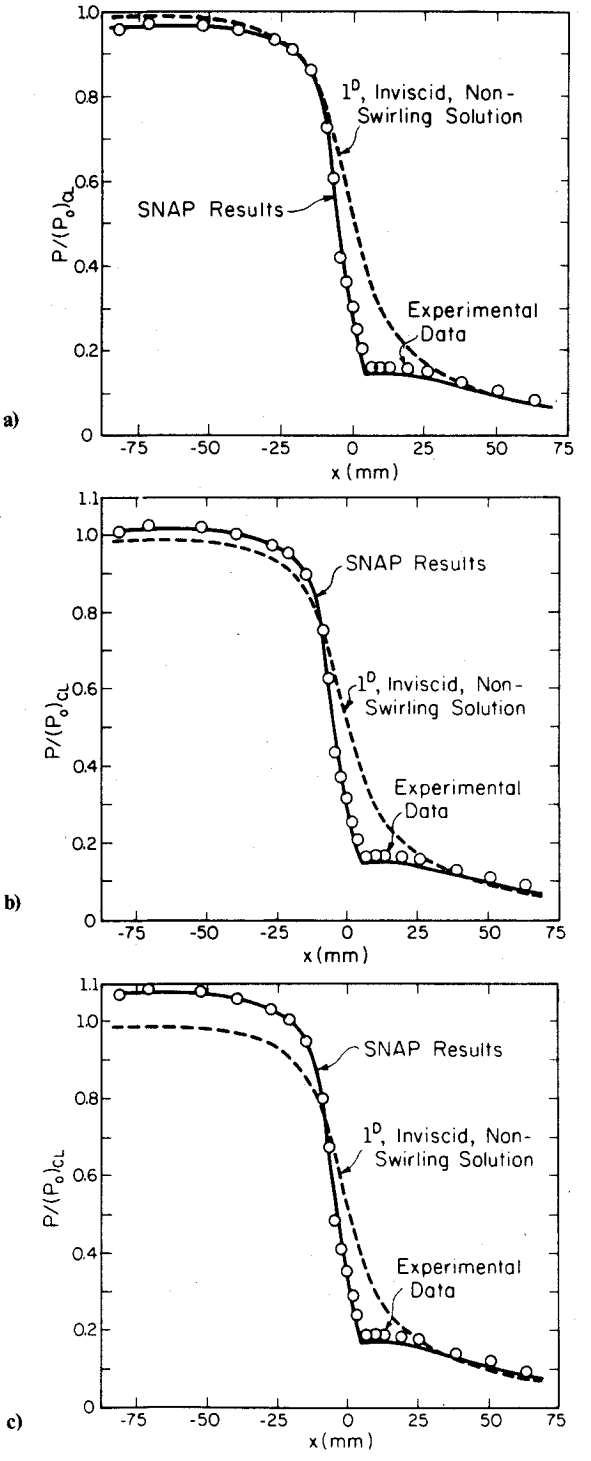

Fig. 12 Comparison of computations with experimental wall static pressure measurements for converging-diverging nozzle flow: a) no swirl; b) CA3 swirler; c) CA5 swirler.

uniform P_0. The results computed for the CA5 case demonstrate that the effect of swirl is significant near the inlet for the wall Mach numbers and for the entire length of the nozzle for the centerline Mach numbers. In contrast to the CA3 case, the Mach numbers for the CA5 swirler are larger than those for no swirl along both the centerline and wall.

The computed and measured wall static pressure distributions are compared in Fig. 12 for the three experimental cases. The static pressures have been nondimensionalized with the stagnation pressure at the nozzle inlet centerline location for each case. As a reference, the conventional, nonswirling, isentropic, one-dimensional solution has also been included.

Table 1 Computed performance parameters for experimental cases

Case	C_D	η_{vs}	η_{SI}	S_i
No swirl	0.9792	0.9501	0.9703	0.0
CA3 swirler	0.9636	0.9355	0.9709	0.3976
CA5 swirler	0.9389	0.9115	0.9708	0.6596

Clearly, the latter solution is in serious disagreement with the data, especially in the throat region. On the other hand, the results computed with the swirling nozzle analysis program ("SNAP") agree very well with the data in all three cases. There is a slight underprediction of the wall pressure immediately downstream of the tangency point between the circular arc throat and conical divergent section ($x=5$ mm). As in previous cases, a weak oblique shock is formed near this location due to Mach wave coalescence. The underprediction may be due to inadequate numerical resolution of the gradients occurring near the tangency point or to a rapid thickening of the wall boundary layer in this region of relatively neutral pressure gradient. The excellent agreement between the numerical and experimental results near the inlet ($x \leq -10$ mm) for the two swirling cases is particularly important since the effects of swirl are most significant in this region.

The computed integral performance parameters for the three experimental cases are presented in Table 1. The specific impulse efficiency is again found to be virtually constant, which is the same result obtained for the previous c-d nozzle geometry. For the CA3 swirler, the discharge coefficient and vacuum stream thrust efficiency are both reduced by about 1.6% over the unswirled case while for CA5 the reduction is about 4.1%. For both swirled cases, the swirl number at the nozzle inlet is significantly higher than the nominal design value at the swirler exit (0.3 and 0.5, respectively). This result is expected since the axial velocity at the swirler exit is higher than that at the nozzle inlet. The swirl angles plotted in Fig. 11b and the inlet swirl numbers given in Table 1 are relatively high, although the reductions in C_D and η_{vs} due to swirl are very moderate. This result is due to the large contraction in area which occurs between the inlet and throat for the experimental nozzle geometry, $A_t/A_i=0.249$. Because of this contraction, the axial velocity at the throat is very much larger than at the inlet, so that the relative effects of swirl at the throat and in the rest of the nozzle are much weaker than at the inlet.

Summary

A time-dependent finite-difference method has been developed to investigate the effects of swirl on supersonic propulsion nozzle performance and flowfield details. The method can be applied to converging, converging-diverging, and annular nozzles with arbitrary inlet distributions of stagnation pressure, stagnation temperature, meridian plane streamline angle, and swirl angle. Example results indicate that significant reductions in the discharge coefficient and vacuum stream thrust efficiency due to swirl may occur, but that the specific impulse efficiency is affected to a far lesser degree. For nozzles without centerbodies, the primary effect of swirl on the flowfield is a strong increase in velocity near the nozzle axis.

A series of experiments has also been performed with a conventional c-d nozzle for a nonswirling and two swirling cases. Measurement of the inlet stagnation pressure and swirl angle profiles shows that, while the inlet flow is reasonably axisymmetric, the inlet P_0 distribution becomes increasingly nonuniform as the swirl level is increased. Excellent agreement between the measured and numerically predicted wall static pressure distributions has also been found for the three experimental cases.

Acknowledgments

This work was sponsored by the Air Force Office of Scientific Research, Contract F49620-82-C-0035, and by the Aero Propulsion Laboratory, Wright-Patterson Air Force Base, OH, Contract F33615-81-C-2078. The author would also like to thank Dr. F. Don Stull, Dr. Roger R. Craig, and the other members of the Ramjet Technology Branch at Wright-Patterson Air Force Base for their assistance with this work.

References

[1]Buckley, P.L., Craig, R.R., Davis, D.L., and Schwartzkopf, K.G., "The Design and Combustion Performance of Practical Swirlers for Integral Rocket/Ramjets," *AIAA Journal*, Vol. 21, May 1983, pp. 733–740.

[2]Carpenter, P.W. and Johannesen, N.H., "An Extension of One-Dimensional Theory to Inviscid Swirling Flow through Choked Nozzles," *Aeronautical Quarterly*, Vol. 26, May 1975, pp. 71–87.

[3]Dutton, J.C., "Analysis of Swirling Nozzle Flow by a Time-Dependent Finite Difference Technique," Mechanical Engineering Department, Texas A&M University, College Station, Rept. TEES-TR-4990-84-01, Dec. 1984.

[4]Guderley, K.G., Tabak, D., Breiter, M.C., and Bhutani, O.P., "Continuous and Discontinuous Solutions for Optimum Thrust Nozzles of Given Length," *Journal of Optimization Theory and Applications*," Vol. 12, Dec. 1973, pp. 588–628.

[5]Boerner, C.J., Sparrow, E.M., and Scott, C.J., "Compressible Swirling Flow through Convergent-Divergent Nozzles," *Wärme- und Stoffübertragung*, Vol. 5, No. 2, 1972, pp. 101–115.

[6]Pandolfi, M., "Transonic Swirling Flow in Axisymmetric Nozzles," *Meccanica*, Vol. 11, Sept. 1976, pp. 157–161.

[7]Kornblum, B.T., Thompson, H.D., and Hoffman, J.D., "An Analytical Investigation of Swirl on Annular Propulsive Nozzles," *Journal of Propulsion and Power*, Vol. 2, March-April 1986, pp. 155–160.

[8]Hoffman, J.D., Thompson, H.D., and Marcum, D.L., "An Analytical Investigation of the Effects of Swirler Design on the Performance of Annular Propulsive Nozzles," AIAA Paper 86-0587, Jan. 1986.

[9]Norton, D.J., Farquhar, B.W., and Hoffman, J.D., "An Analytical and Experimental Investigation of Swirling Flow in Nozzles," *AIAA Journal*, Vol. 7, Oct. 1969, pp. 1992–2000.

[10]Dunlap, R., "An Investigation of the Swirling Flow in a Spinning End-Burning Rocket," *AIAA Journal*, Vol. 7, Dec. 1969, pp. 2293–2300.

[11]Batson, J.L. and Sforzini, R.H., "Swirling Flow through a Nozzle," *Journal of Spacecraft and Rockets*, Vol. 7, Feb. 1970, pp. 159–163.

[12]Sforzini, R.H. and Essing, J.E., "Swirling Flow through Multiple Nozzles," *Journal of Spacecraft and Rockets*, Vol. 7, Nov. 1970, pp. 1366–1369.

[13]Cline, M.C., "VNAP: A Computer Program for Computation of Two-Dimensional, Time-Dependent, Compressible, Viscous, Internal Flow," Los Alamos Scientific Laboratory, Los Alamos, NM, Rept. LA-7326, Nov. 1978.

[14]MacCormack, R.W., "The Effect of Viscosity in Hypervelocity Impact Cratering," AIAA Paper 69-354, April 1969.

[15]Dutton, J.C., "Time-Dependent Calculations of Swirling Nozzle Flow," Final Report for 1983 USAF-SCEEE Summer Faculty Research Program, Contract F49620-82-C-0035, Aug. 1983.

[16]Bresnahan, D.L. and Johns, A.L., "Cold Flow Investigation of a Low Angle Turbojet Plug Nozzle with Fixed Throat and Translating Shroud at Mach Numbers from 0 to 2.0," NASA TM X-1619, Aug. 1968.

[17]Craig, R.R. and Buckley, P.L., Ramjet Technology Branch, Wright-Patterson Air Force Base, Dayton, OH, private communication, Sept. 1984.